Fuel-Optimal Powered Descent Guidance for Hazardous Terrain

Sheikh Zeeshan Basar * **Satadal Ghosh** **

* *Department of Aerospace Engineering, Indian Institute of Technology, Madras, India (e-mail: ae21s013@smail.iitm.ac.in).*
** *Room 222, CTC Building, Department of Aerospace Engineering, Indian Institute of Technology, Madras, India (e-mail: satadal@iitm.ac.in)*

Abstract: Future interplanetary missions will carry more and more sensitive equipment critical for setting up bases for crewed missions. The ability to manoeuvre around hazardous terrain thus becomes a critical mission aspect. However, large diverts and manoeuvres consume a significant amount of fuel, leading to less fuel remaining for emergencies or return missions. Thus, requiring more fuel to be carried onboard. This work presents fuel-optimal guidance to avoid hazardous terrain and safely land at the desired location. We approximate the hazardous terrain as step-shaped polygons and define barriers around the terrain. Using an augmented cost functional, fuel-optimal guidance command, which avoids the terrain, is derived. The results are validated using computer simulations and tested against many initial conditions to prove their effectiveness.

Keywords: Aerospace, Space exploration and transportation, Guidance, navigation and control of vehicles, Autonomous systems

1. INTRODUCTION

While the first moon landing (Luna 2 by erstwhile-Soviet Union in 1959) was an intentional hard impact, and due to scientists and engineers worldwide, uncrewed missions to several planets and other celestial bodies in our solar system have succeeded. An essential requirement in all these missions is to receive data back, for which the spacecraft must survive the landing. A typical soft landing on a rocky planet has four key stages: 1. orbital injection, 2. hypersonic entry, 3. parachute descent, and finally, 4. powered descent. While the parachute descent stage can reduce the spacecraft's velocity to subsonic speed, it is not enough. Further, during the powered descent stage, the guidance law must be robust to perturbation, consume the least fuel, and land softly as close to the desired site as possible. Today, another critical mission requirement is to bring the samples back to Earth for further analysis. Such mission requirements place greater importance on the fuel-optimality aspect of a powered descent. The study of autonomous guidance laws for powered descent began with the Apollo era. However, most guidance laws were rudimentary, as they were severely limited by the computational power and memory. In fact, the Apollo missions used a straightforward polynomial-based guidance law (Klumpp (1974)). The polynomial-based guidance is relatively easier to implement; however, they lack in fuel-optimality, robustness and the required accuracy.

Since the late 1990s, significant efforts have been made to ensure fuel optimality. As computing power readily increases, numerical optimisation methods have come into the spotlight. Particularly convex optimisation methods have gained popularity in both research and industry due to the theoretical assurances and computational performance they provide, and can be used to find optimal, and accurate solutions to the ideal powered descent problem as well. However, realistic missions have nonconvexities due to thrust constraints, nonlinear dynamics, and coupled state-control dynamics. To address these nonconvexities, algorithms such as Lossless Convexification (LCvx) and Successive Convexification (SCvx) have been developed (Açikmeşe and Ploen (2007), Açikmeşe and Blackmore (2011), Blackmore et al. (2012), Mao et al. (2016), Mao et al. (2018)). These algorithms have been successfully used for powered descent problems. However, convexification-based methods are open-loop and, therefore, highly susceptible to perturbations and estimation errors. Feedback guidance laws have been presented in the literature to alleviate the abovementioned issues. Classical feedback laws for missile guidance, like Proportional Navigation (PNG) as discussed in Zarchan (2012), have inspired some of the earliest guidance laws for autonomous landing. Several variations of PNG exists and its adaptations such as biased-PNG (Kim et al. (1998)) and pulsed-PNG (Wie (1998)), have been explored for powered descent. Extending the idea of zero-effort-miss (ZEM) in missile guidance laws to include the deviations in velocity Ebrahimi et al. (2008) proposed the idea of zero-effort-velocity (ZEV), and using Pontryagin's Maximum Principle (Pontryagin et al. (1986)), fuel optimal guidance law was developed as a function of ZEM and ZEV.

Utilising the core idea of ZEM/ZEV-based optimal guidance law, powered descent was made robust against perturbations using Sliding Mode Control, and its variants (Furfaro et al. (2011), Furfaro et al. (2013b), Wibben and Furfaro (2016), Furfaro et al. (2013a)). Missile guidance

concepts, such as collision course and heading error, further inspired the work in Shincy and Ghosh (2021) to develop a novel SMC-based guidance law in full nonlinear setting. The work was then extended to include fuel optimality as well in Shincy and Ghosh (2022).

A critical drawback of the optimal guidance law is that a part of the trajectory is underground for a large terminal time, which is not desirable. One can try to lower the terminal time, but it requires a significantly larger thrust command to succeed. Optimal sliding guidance laws attempt to obviate these issues, but the efficacy heavily depends on the choice of terminal time and sliding mode constants. There are methods discussed in Guo et al. (2012) to determine the optimal terminal time analytically. However, the expression is a quartic polynomial which is computationally expensive to solve. In the same work, the idea of using waypoints to avoid crashing into the planetary surface was also introduced, which was later extended in Guo et al. (2013) to choose the waypoint optimally. The optimal waypoint method can quickly become computationally expensive as the number of time steps increases and if both terminal and waypoint times are left free for the optimiser to solve.

By including a switching-form term that was relevant to the lander's position, Zhou and Xia (2014) proposed an improved ZEM/ZEV feedback guidance for the Mars powered descent phase. This guidance was effective with good performance in avoiding collisions, but the added term mainly relies on expert experience, which may reduce reliability to some extent and cannot ensure the near fuel optimality. Zhang et al. (2017) proposed a self-adjusting augmentation to the performance index to obviate these issues, and the developed guidance law was not heavily dependent on the guidance law designer. The novel guidance law was then found to be near-fuel-optimal, proved using Monte Carlo simulations against the classical ZEM/ZEV guidance.

Most of the existing literature consider the terrain around the landing site to relatively flat, and go only as far as using simple glideslope constraints to avoid minor undulation and debris near the surface. To attempt landing at treacherous terrain, glideslope constraints may be too conservative. To allow for more freedom of motion for the lander, terrain avoidance guidance was first presented by Gong et al. (2021), where Barrier Lyapunov Functions were used to avoid crashing into the terrain. Gong et al. (2022) then explored terrain avoidance using prescribed performance functions. Both guidance laws were able to avoid crashing into terrain and safely land. However, the guidance law developed requires rate information to be estimated. Further, the fuel optimality and performance under thrust constraints were not investigated.

Optimal Terrain Avoidance Landing Guidance (OTALG) is presented in this paper to land safely at the desired site while avoiding terrain and maintaining near-fuel optimality. The terrain is approximated as n step-shaped polygons, using readily available terrain data. We then introduce the barrier polynomials which bound the terrain, based on the dimensions of the step-shaped polygons. A novel augmentation to the performance index is introduced next, which introduces penalty if the lander moves close to the barriers. Fuel optimal guidance law is developed as a function of $\mathbf{ZEM}(t)$ and $\mathbf{ZEV}(t)$. Both can be calculated online, given the lander's current position and velocity, t_{go} and the terminal conditions. The main goal of this work is to demonstrate that the lander can safely manoeuvre in presence of terrain, softly land at the desired landing site, and most importantly maintain near-fuel optimality. The efficacy of our work in terrain avoidance shown using computer simulations. Using Monte Carlo simulations, we demonstrate near-fuel optimality of the proposed guidance law. To the best of author's knowledge, the proposed guidance law is the first attempt at *fuel optimal*, terrain avoidance guidance law for powered descent.

The rest of the paper is organised as follows. Section 2 details the landing dynamics and some preliminaries from the optimal control theory. Then using piecewise-smooth polynomials and information about the terrain, barriers are developed in Section 3. Section 4 introduces the terrain avoidance performance index, and the optimal guidance law is derived subsequently. Section 5 presents the simulation results and some discussions on some of the issues that need to be addressed. Finally, the work is concluded in Section 6, with some remarks on the plan of action going forward.

2. PROBLEM FORMULATION AND PRELIMINARIES

For our problem, we choose the non-rotating, inertial ENU-frame with origin at the landing site as in Fig. 1. Assuming a 3-DOF dynamics, the lander can be modelled as:

$$\begin{aligned} \dot{\mathbf{r}} &= \mathbf{v} \\ \dot{\mathbf{v}} &= \mathbf{a} + \mathbf{g} + \mathbf{a}_{\text{p}} \\ \mathbf{a} &= \frac{\mathbf{T}}{m} \\ \dot{m} &= -\frac{\|\mathbf{T}\|}{I_{\text{sp}} g_e} \end{aligned} \tag{1}$$

where, $\mathbf{r} = [r_x, r_y, r_z]^{\text{T}}$ represents the position, $\mathbf{v} = [v_x, v_y, v_z]^{\text{T}}$ represents the velocity, and $\mathbf{g} = [g_x, g_y, g_z]^{\text{T}}$ is the local gravity. The guidance command provided by the thrusters is represented by $\mathbf{a} = [a_x, a_y, a_z]^{\text{T}}$, $\mathbf{a}_p$ is the net acceleration caused due to bounded perturbations (e.g. wind), m is the lander's mass, I_{sp} is the specific impulse, and g_e is the gravitational acceleration of Earth. Since the altitude at which the powered descent stage starts is significantly smaller than the radius of planets, it is valid to assume a constant gravitational acceleration acting only along the z-axis, that is, $\mathbf{g} = [0, 0, g]^{\text{T}}$.

The core idea of ZEM and ZEV is to determine the deviation from the desired position ($\mathbf{r}_f$) and velocity ($\mathbf{v}_f$) at the final time t_f if no control effort is applied from current time t. Defining time-to-go, $t_{\text{go}} \triangleq t_f - t$, we have:

$$\begin{aligned} \mathbf{ZEM}(t) &= \mathbf{r}_f - \left[\mathbf{r}(t) + \mathbf{v} t_{\text{go}} + \frac{1}{2}\mathbf{g} t_{\text{go}}^2\right] \\ \mathbf{ZEV}(t) &= \mathbf{v}_f - \left[\mathbf{v}(t) + \mathbf{g} t_{\text{go}}\right] \end{aligned} \tag{2}$$

where, $\mathbf{r}(t_f)$, and $\mathbf{v}(t_f)$ represent the position and velocity at the final time.

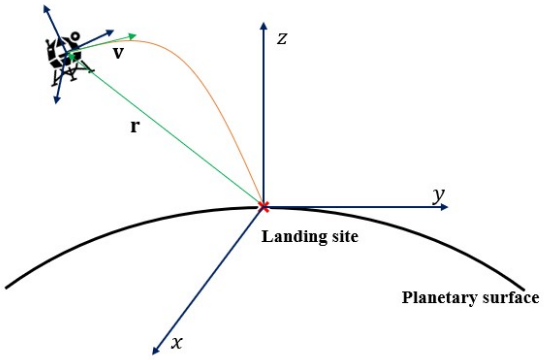

Fig. 1. Landing Dynamics

The classical ZEM/ZEV-based optimal guidance law of Ebrahimi et al. (2008) is derived by considering the performance index as:

$$J = \frac{1}{2}\int_{t_0}^{t_f} \mathbf{a}^{\mathrm{T}}\mathbf{a}\, dt, \tag{3}$$

subjected to the dynamics in (1), with $\mathbf{a}_{\mathrm{p}} = 0$. The guidance law is then

$$\mathbf{a} = \frac{6}{t_{\mathrm{go}}^2}\mathbf{ZEM}(t) - \frac{2}{t_{\mathrm{go}}}\mathbf{ZEV}(t). \tag{4}$$

3. BARRIER DEFINITION AROUND HAZARDOUS TERRAIN

Terrain data available from reconnaissance missions can be used to create the n-step-shaped polygons to approximate the terrain, as shown in Fig. 2. Defining the height of j^{th} step as $h_{i,j}$, and the horizontal distance from the landing site (origin) along i-axis as $w_{i,j}$, where $i = x,\, y$.

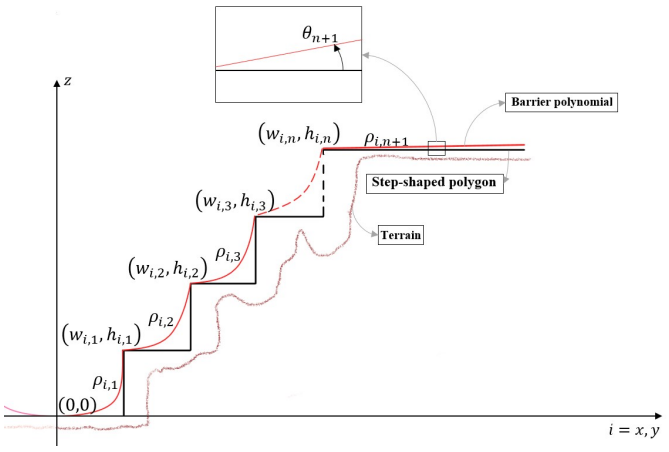

Fig. 2. Illustration of terrain and barrier around n-step shaped polygons.

3.1 Barriers for horizontal motion

To restrict the motion in the horizontal planes, we define a barrier polynomial $\rho_{i,j}$ as in (5). For n-steps, we will define $n+1$ number of barriers, where the order of the polynomial is determined on the basis of degree of conservatism the mission demands. A higher degree polynomial will closely hug the step shape, allowing for more freedom of movement for the lander. We further consider the $(n+1)^{\text{th}}$ barrier to be a linear polynomial instead of any higher order polynomial to reduce conservatism.

$$\rho_{i,j} = \begin{cases} \pm\left(\beta_{i,j}(r_z + \gamma_{i,j})^{\frac{1}{\lambda_{i,j}}} + \alpha_{i,j}\right), & h_{i,(j-1)} \le r_z \le h_{i,j} \\ \pm\left(\beta_{i,(n+1)}(r_z + \gamma_{i,(n+1)}) + \alpha_{i,(n+1)}\right), & r_z \ge h_{i,n} \end{cases} \tag{5}$$

where $i = x,\, y$ and $j = 1, \ldots, n$. From the first barrier to the n^{th} barriers, the constants are defined as:

$$\begin{aligned} \alpha_{i,j} &= w_{i,(j-1)} \\ \beta_{i,j} &= \frac{w_{i,j} - w_{i,(j-1)}}{\left(h_{i,j} - h_{i,(j-1)}\right)^{\frac{1}{\lambda_{i,j}}}} \\ \gamma_{i,j} &= -h_{i,(j-1)} \end{aligned} \tag{6}$$

and $\lambda_{i,j}$ is a positive, even natural number. Further note that, $h_{i,0} = 0$, and $w_{i,0} = 0$, that is, the landing site (origin). For the $(n+1)^{\text{th}}$ barrier, we first choose the slope angle of the barrier, $\theta_{(n+1)}$ with respect to the axis under consideration. The angle can be chosen as a small value (approx. $0.05^\circ - 0.1^\circ$) for a relatively flat plateau or can be chosen to be larger for scenarios where a hill precedes a canyon precedes the landing site. The constants can now be defined as:

$$\begin{aligned} \alpha_{i,(n+1)} &= w_{i,n} \\ \beta_{i,(n+1)} &= \tan\left(\frac{\pi}{2} - \theta_{(n+1)}\right) \\ \gamma_{i,(n+1)} &= -h_{i,n} \end{aligned} \tag{7}$$

3.2 Barriers for vertical motion

It is imperative to define barriers at specific heights to avoid crash landing into the terrain due to vertical motion. We do this by including a small margin, δ, to the height of the next lower barrier. The designer can choose this margin of safety as per requirement. However, here we run into the problem that if the lander is within the lateral bound of j^{th} step but is above the height of $(j+1)^{\text{th}}$ step, the lander keeps bouncing off the vertical barrier of $(j+1)^{\text{th}}$. To address this issue, we select the vertical barrier using the following simple comparison:

$$\rho_{z,j} = \begin{cases} h_n + \delta, & r_z \ge h_{i,n} \\ h_j + \delta, & \left(h_{i,j} \le r_z \le h_{i,(j-1)}\right) \text{ AND} \\ & \left(w_{i,j} \le \|[r_x,\, r_y]^{\mathrm{T}}\|_\infty \le w_{i,(j-1)}\right) \end{cases} \tag{8}$$

where $j = 1, \ldots, n$.

4. DEVELOPMENT OF FEEDBACK GUIDANCE

In this section we discuss the development of the feedback guidance law, which can navigate the terrain and land safely at the desired landing site, while consuming least amount of fuel.

4.1 Performance index for collision avoidance

To avoid crashing into the local terrain, we introduce a novel augmentation to the performance index.

$$J = \int_0^{t_f} \left[\mathbf{a}^{\mathrm{T}}\mathbf{a} - \sum_i l_{3,i} e^{-\phi_i} \right] d\tau \tag{9}$$

where, $i = x, y, z$, $l_{3,i} > 0$ is a constant, and $e^{-\phi_i}$ is the augmentation term where ϕ_i is defined as:

$$\phi_i = \frac{l_{2,i}}{d_i^2 + l_{1,i}}$$

where, $d_i = r_i - \rho_{i,j}$. Physically, d_i represents how far the lander is with respect to the barrier polynomial. When the lander is farther away from the barriers, the augmentation is large and positive, so the term inside the integration in (9) is small. When the lander is close to the barrier, the augmentation is almost zero, increasing the cost. This penalty generates an acceleration command in direction opposite to the direction of motion to avoid crashing into terrain.

4.2 Guidance law

Based on the proposed performance index and the barrier definition around the terrain, we use methods from optimal control theory to develop the guidance command. Starting with the performance index in (9), we subject it to the dynamics in (1), with $\mathbf{a}_{\mathrm{p}} = 0$. The Hamiltonian is written as:

$$H = \frac{1}{2}\left[\mathbf{a}^{\mathrm{T}}\mathbf{a} - \sum_i l_{3,i} e^{-\phi_i} \right] + \mathbf{p}_r^{\mathrm{T}}\mathbf{v} + \mathbf{p}_v^{\mathrm{T}}(\mathbf{a} + \mathbf{g}). \tag{10}$$

Since (10) is not linear in $\mathbf{a}$, the optimal control is of the form:

$$\frac{\partial H}{\partial \mathbf{a}} = 0 \Rightarrow \mathbf{a} = -\mathbf{p}_v. \tag{11}$$

For the dynamics (1), the co-states are:

$$\dot{\mathbf{p}}_r = \frac{\partial}{\partial \mathbf{r}}\left[\frac{1}{2}\sum_i l_{3,i} e^{-\phi_i} \right] \tag{12}$$

$$\dot{\mathbf{p}}_v = -\mathbf{p}_r \tag{13}$$

From (12):

$$\dot{p}_{r_x} = \frac{1}{2}\left[\sum_i l_{3,i} \frac{\partial \phi_i}{\partial r_x} \mathrm{e}^{-\phi_i} \right]$$

$$\Rightarrow \dot{p}_{r_x} = l_{2,x} l_{3,x} \frac{d_x \mathrm{e}^{-\phi_x}}{\left(d_x^2 + l_{1,x}\right)^2}$$

$$\Rightarrow \dot{p}_{r_i} = l_{2,i} l_{3,i} \frac{d_i \mathrm{e}^{-\phi_i}}{\left(d_i^2 + l_{1,i}\right)^2}. \tag{14}$$

$$\text{Defining, } \mathbf{p} \triangleq [\dot{p}_{r_x}, \dot{p}_{r_y}, \dot{p}_{r_z}] \tag{15}$$

From (12) and (15), we can solve for $\mathbf{p}_r$:

$$\dot{\mathbf{p}}_r = \mathbf{p}$$

$$\Rightarrow \mathbf{p}_{\mathrm{rf}} - \mathbf{p}_r = \mathbf{p} t_{\mathrm{go}}$$

$$\Rightarrow \mathbf{p}_r = \mathbf{p}_{\mathrm{rf}} - \mathbf{p} t_{\mathrm{go}} \tag{16}$$

where $\mathbf{p}_{\mathrm{rf}} = \mathbf{p}_r(t_f)$.
Solving for $\mathbf{p}_v$ using (13) and (16):

$$\dot{\mathbf{p}}_v = \mathbf{p} t_{\mathrm{go}} - \mathbf{p}_{\mathrm{rf}}$$

$$\Rightarrow \mathbf{p}_{\mathrm{vf}} - \mathbf{p}_v = \mathbf{p}\frac{t_{\mathrm{go}}^2}{2} - \mathbf{p}_{\mathrm{rf}} t_{\mathrm{go}}$$

$$\Rightarrow \mathbf{p}_v = \mathbf{p}_{\mathrm{vf}} + \mathbf{p}_{\mathrm{rf}} t_{\mathrm{go}} - \mathbf{p}\frac{t_{\mathrm{go}}^2}{2} \tag{17}$$

where $\mathbf{p}_{\mathrm{vf}} = \mathbf{p}_v(t_f)$.
Finally, from (11)

$$\mathbf{a} = -\mathbf{p}_{\mathrm{vf}} - \mathbf{p}_{\mathrm{rf}} t_{\mathrm{go}} + \mathbf{p}\frac{t_{\mathrm{go}}^2}{2} \tag{18}$$

Expressions for position and velocity can be obtained by substituting (18) in the dynamics and integrating.

$$\mathbf{r} = \mathbf{r}_f - \mathbf{v}_f t_{\mathrm{go}} - (\mathbf{p}_{\mathrm{vf}} - \mathbf{g})\frac{t_{\mathrm{go}}^2}{2} - \mathbf{p}_{\mathrm{rf}}\frac{t_{\mathrm{go}}^3}{6} + \mathbf{p}\frac{t_{\mathrm{go}}^4}{24} \tag{19}$$

$$\mathbf{v} = \mathbf{v}_f + (\mathbf{p}_{\mathbf{vf}} - \mathbf{g})\, t_{\mathrm{go}} + \mathbf{p}_{\mathrm{rf}}\frac{t_{\mathrm{go}}^2}{2} - \mathbf{p}\frac{t_{\mathrm{go}}^3}{6} \tag{20}$$

Solving for terminal co-states:

$$\mathbf{p}_{\mathrm{rf}} = \frac{12}{t_{\mathrm{go}}^3}\left[(\mathbf{r} - \mathbf{r}_f) + (\mathbf{v} + \mathbf{v}_f)\frac{t_{\mathrm{go}}}{2} + \mathbf{p}\frac{t_{\mathrm{go}}^4}{24} \right] \tag{21}$$

$$\mathbf{p}_{\mathrm{vf}} = -\frac{6}{t_{\mathrm{go}}^2}\left[(\mathbf{r} - \mathbf{r}_f) + (\mathbf{v} + 2\mathbf{v}_f)\frac{t_{\mathrm{go}}}{3} + \mathbf{p}\frac{t_{\mathrm{go}}^4}{72} \right] + \mathbf{g} \tag{22}$$

Finally, substituting (21), and (22) in the expression for acceleration in (18), we get the optimal guidance command as:

$$\mathbf{a}_{\mathrm{OTALG}} = \frac{6}{t_{go}^2}\mathbf{ZEM}(t) - \frac{2}{t_{\mathrm{go}}}\mathbf{ZEV}(t) + \mathbf{p}\frac{t_{\mathrm{go}}^2}{12} \tag{23}$$

4.3 Analysis

Defining a new vector $\mathbf{\Gamma} \triangleq [p_x\frac{t_{\mathrm{go}}^2}{12}, p_y\frac{t_{\mathrm{go}}^2}{12}, p_z\frac{t_{\mathrm{go}}^2}{12}]^{\mathrm{T}}$, which is the collision avoidance term in (23). Taking partial derivative of Γ_i with respect to the corresponding direction

$$\frac{\partial \Gamma_i}{\partial r_i} = \frac{\kappa}{(d_i^2 + l_{1,i})^2}\left[1 - \frac{4d_i^2}{(d_i^2 + l_{1,i})} + \frac{2l_{2,i}d_i^2}{(d_i^2 + l_{1,i})^2} \right] e^{-\phi_i} \tag{24}$$

where $\kappa = \dfrac{l_{2,i} l_{3,i} t_{\mathrm{go}}^2}{12}$. The non-trivial critical points of (24) are when $e^{-\phi_i} = 0$, or $1 - \dfrac{4d_i^2}{(d_i^2 + l_{1,i})} + \dfrac{2l_{2,i}d_i^2}{(d_i^2 + l_{1,i})^2} = 0$. Considering the structure of ϕ_i, the former does not have real solutions, so only the latter condition must be checked to determine the critical points. Simplifying the latter condition, we get the critical values of d_i as:

$$d_i^* = \pm\frac{\sqrt{\sqrt{l_{2,i}^2 - 2l_{1,i}l_{2,i} + 4l_{1,i}^2} + l_{2,i} - l_{1,i}}}{\sqrt{3}}. \tag{25}$$

The maximum divert acceleration occurs at d_i^*, which is the critical distance of the barrier to the lander. The safety margin must be chosen while keeping point of maximum divert and the thrust constraints in mind. From (25), it is clear that $l_{1,i}$, and $l_{2,i}$ directly affect the safety margin, and from (23) $l_{3,i}$ has the most significant effect on the magnitude of the divert.

From a design perspective, knowledge of the maximum thrust the guidance law needs is a prerequisite. We look at the performance index (9) to determine $T_{i_{\max}}$ where $i = x, y, z$. To ensure $J > 0$, the following must hold:

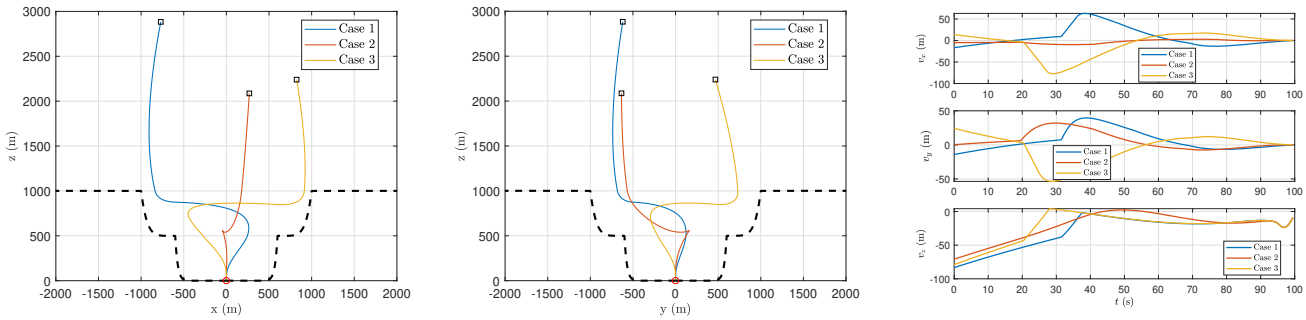

(a) Trajectories in $x - z$ plane. (b) Trajectories in $y - z$ plane. (c) Velocity profiles

Fig. 3. Trajectories and velocity profile.

$$a_{i_{\max}}^2 - l_{3,i}\mathrm{e}^{-\phi_i} \geq 0$$
$$\Rightarrow |a_{i_{\max}}| \geq \sqrt{l_{3,i}\mathrm{e}^{-\phi_i}} \tag{26}$$

From (26), we get:

$$|T_{i_{\max}}| \geq m_0\sqrt{l_{3,i}\mathrm{e}^{-\phi_i}} \tag{27}$$

4.4 Some remarks

While we have not investigated the effects of thrust constraints in detail, some comments can be made at this stage. We consider the thrust constraint of the form:

$$0 \leq \|\mathbf{T}\| \leq T_{\max} \tag{28}$$

(1) The safety margin must be chosen such that, $\delta > d_i^*$.
(2) Considering $l_{1,i} \geq 0$, and $l_{2,i} \geq 1$, we can fix $l_{1,i}$ and choose $l_{2,i} \gg l_{1,i}$.
(3) Further, a large $l_{3,i} \gtrapprox 200$ should be chosen.

5. SIMULATIONS

Considering the landing scenario in a Martian environment, simulations are presented to demonstrate the effectiveness of the proposed guidance law. A simplified version of simulation parameters of Açikmeşe and Ploen (2007) have been considered for simulation. We assume a point-mass lander with specific impulse $I_{\text{sp}} = 225$ s and $T_{\max} = 31000$ N (equivalent to ten thrusters, each with 3100 N max thrust). The terminal conditions are $\mathbf{r}_f = [0, 0, 0]^{\mathrm{T}}$ m, $\mathbf{v}_f = [0, 0, 0]^{\mathrm{T}}$ m/s, at $t_f = 100$ s. The simulation is stopped when $r_z = 0.05$ m or terminal time is achieved, whichever occurs first. To portray the effectiveness of our guidance law in avoiding hazardous terrain and fuel optimality, we sample initial conditions from a normally distributed set as prescribed in Table 1. We compare the fuel-optimality of our guidance law with the guidance laws presented in Ebrahimi et al. (2008) and Zhang et al. (2017). Further, the fuel consumption is also tested under atmospheric perturbations modelled as

$$\mathbf{a}_p(t) = 0.5\mathbf{a}_{\text{OTALG}} \sin\left(\frac{\pi}{3}t\right). \tag{29}$$

To emulate a trench surrounding the landing site on Mars, we consider the terrain that can be modelled as a 2-step, flat-top shape. The height and width from the origin of each step are given in Table 3. To design the barriers, we choose $\theta_3 = 0.05°$, with $\lambda_{i,2} = 6$, and $\lambda_{i,1} = 20$. Further, the margin of safety in the vertical barrier is $\delta = 1.2d_i^*$. The guidance law constant are chosen as $l_{1,i} = 1$, $l_{2,i} = 3000$, and $l_{3,i} = 280$. Finally, the local gravity at Mars is assumed to be $g = [0,\ 0,\ -3.7114]^{\mathrm{T}}$ m/s^2, and acceleration due to gravity on Earth $g_e = 9.807$ m/s^2.

Table 1. Initial Conditions Distribution Setup

Initial Condition	μ	σ^2
x_0 (m)	-800, 0, 800	350
y_0 (m)	-800, 0, 800	350
z_0 (m)	2500	500
$v_{\text{x}0}$ (m/s)	-25, 0, 25	10
$v_{\text{y}0}$ (m/s)	-25, 0, 25	10
$v_{\text{z}0}$ (m/s)	-80	10
m_0 (kg)	1900, 2100	100

5.1 Terrain collision avoidance

From the distribution in Table 1, $N = 3$ samples are chosen (shown in Table 2) of which the trajectories are shown in Fig. 3a, and Fig. 3b. The velocity profile is shown in Fig. 3c.

Table 2. Initial Conditions

Case #	$\mathbf{r}_0$	$\mathbf{v}_0$	m_0
Case 1	$[-769.42, -619.63, 2883.33]^{\mathrm{T}}$	$[-16.78, -14.08, -83.36]^{\mathrm{T}}$	1961.80
Case 2	$[269.35, -634.30, 2086.65]^{\mathrm{T}}$	$[-4.98, 0.29, -70.89]^{\mathrm{T}}$	1916.55
Case 3	$[823.91, 467.70, 2240.03]^{\mathrm{T}}$	$[13.81, 24.28, -79.47]^{\mathrm{T}}$	1959.43

First and foremost, it is clear that the guidance law brings the lander softly to the landing site. There are no sudden jerks in either the trajectories or the velocity profiles. We can observe the guidance law working to avoid the terrain from the trajectory figures and the velocity profiles. Consider Case 3 in Fig. 3a. When the lander is near the terrain, the acceleration command generated by the collision avoidance term pushes it away from the terrain by changing the velocity direction, as clearly observed in the v_x plot of Fig. 3c. In all three cases as the lander comes towards the landing site, the proposed guidance law generates the acceleration in the direction opposite to the direction of motion, and softly reaches the landing site.

5.2 Fuel consumption

We compare the proposed terrain avoidance guidance law (Algorithm 1) to the work done in Zhang et al. (2017)

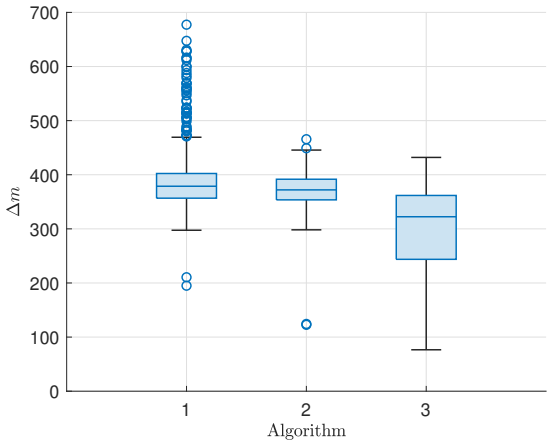

(a) Fuel consumption statistics

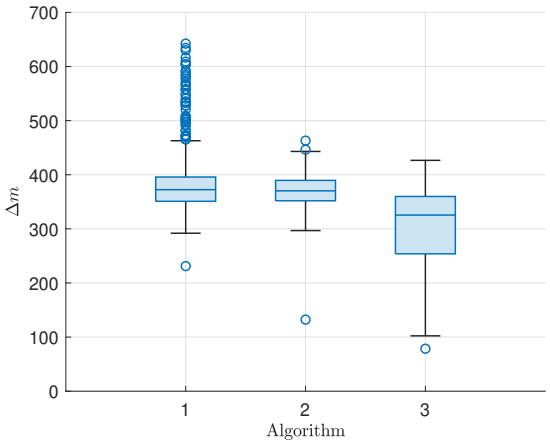

(b) Fuel consumption statistics with a_p

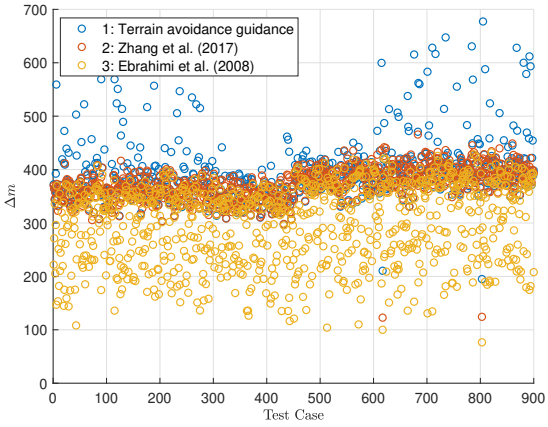

(c) Fuel consumption

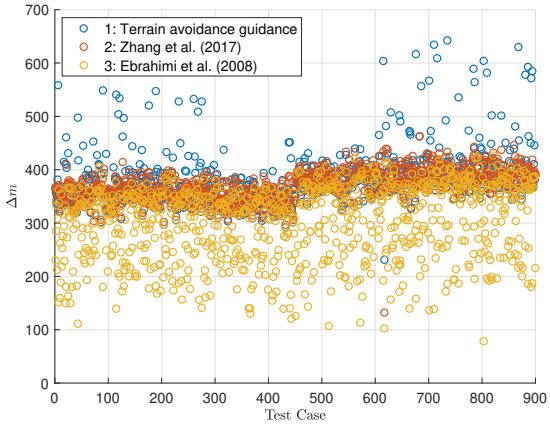

(d) Fuel consumption with a_p

Fig. 4. Simulations results on fuel consumption

Table 3. Terrain model

	Height (m)	Width (m)
Step-1	500	600
Step-2	1000	1000

(Algorithm 2) and Ebrahimi et al. (2008) (Algorithm 3) as they have been shown to be near fuel optimal. Using the data in Table 1 we generate $N = 900$ initial conditions and run all three guidance laws. The terrain setup and guidance law constants are the same as in the previous subsection. The median fuel consumption (shown in Fig. 4a) is slightly higher for our guidance law, which is expected due to the lander trying to manoeuvre away from the terrain. Figure 4c shows the fuel consumption in all three guidance laws. The data points between $\Delta m \approx 500$ kg to $\Delta m \approx 700$ kg represent the cases requiring more manoeuvres to avoid collisions. Under the same initial conditions, the fuel optimality is again preserved when perturbation in (29) is also included. The results are in Fig. 4b, and Fig. 4d.

6. CONCLUSION

Optimal guidance law for fuel-optimal, hazardous terrain landing has been presented. The terrain has been modelled as n-step-shaped polygons, and barriers have been defined over the terrain model using piecewise-smooth polynomials. Considering terrain avoidance as a penalty on the running cost, fuel optimal guidance law has been derived. The efficacy of the guidance law is tested in a trench in the Martian environment, emulated using a flat-top, 2-step shape. The terrain avoidance guidance successfully avoids the terrain. Using extensive simulations, the near-fuel optimality is confirmed. The guidance law avoids terrain under bounded perturbation and maintains near-fuel optimality. As a part of future work, the thrust constraints need to be investigated in greater detail. Specific corner cases need to investigated, and the barrier polynomial can be made more smooth. Finally, the robustness of the terrain avoidance guidance needs to be investigated.

REFERENCES

Açikmeşe, B. and Blackmore, L. (2011). Lossless convexification of a class of optimal control problems with non-convex control constraints. *Automatica*, 47.

Açikmeşe, B. and Ploen, S.R. (2007). Convex programming approach to powered descent guidance for mars landing. *Journal of Guidance, Control, and Dynamics*, 30.

Blackmore, L., Açıkmeşe, B., and Carson, J.M. (2012). Lossless convexification of control constraints for a class

of nonlinear optimal control problems. *Systems and Control Letters*, 61.

Ebrahimi, B., Bahrami, M., and Roshanian, J. (2008). Optimal sliding-mode guidance with terminal velocity constraint for fixed-interval propulsive maneuvers. *Acta Astronautica*, 62.

Furfaro, R., Cersosimo, D., and Wibben, D.R. (2013a). Asteroid precision landing via multiple sliding surfaces guidance techniques. *Journal of Guidance, Control, and Dynamics*, 36.

Furfaro, R., Gaudet, B., Wibben, D.R., Kidd, J., and Simo, J. (2013b). Development of non-linear guidance algorithms for asteroids close-proximity operations. In *AIAA Guidance, Navigation, and Control (GNC) Conference*.

Furfaro, R., Selnick, S., Cupples, M., and Cribb, M. (2011). Non-linear sliding guidance algorithms for precision lunar landing. *Advances in the Astronautical Sciences*, 140.

Gong, Y., Guo, Y., Ma, G., Zhang, Y., and Guo, M. (2021). Barrier lyapunov function-based planetary landing guidance for hazardous terrains. *IEEE/ASME Transactions on Mechatronics*.

Gong, Y., Guo, Y., Ma, G., Zhang, Y., and Guo, M. (2022). Prescribed performance-based powered descent guidance for step-shaped hazardous terrains. *IEEE Transactions on Aerospace and Electronic Systems*, 58.

Guo, Y., Hawkins, M., and Wie, B. (2012). Optimal feedback guidance algorithms for planetary landing and asteroid intercept. *AAS/AIAA astrodynamics specialist conference*, 142.

Guo, Y., Hawkins, M., and Wie, B. (2013). Waypoint-optimized Zero-Effort-Miss/Zero-Effort-Velocity feedback guidance for mars landing. *Journal of Guidance, Control, and Dynamics*, 36.

Kim, B.S., Lee, J.G., and Han, H.S. (1998). Biased PNG law for impact with angular constraint. *IEEE Transactions on Aerospace and Electronic Systems*, 34.

Klumpp, A.R. (1974). Apollo lunar descent guidance. *Automatica*, 10.

Mao, Y., Szmuk, M., and Açıkmeşe, B. (2016). Successive convexification of non-convex optimal control problems and its convergence properties. In *2016 IEEE 55th Conference on Decision and Control (CDC)*.

Mao, Y., Szmuk, M., Xu, X., and Açikmese, B. (2018). Successive convexification: A superlinearly convergent algorithm for non-convex optimal control problems. *arXiv preprint arXiv:1804.06539*.

Pontryagin, L.S., Neustadt, L.W., and Pontryagin, L.S. (1986). *The mathematical theory of optimal processes*. Gordon and Breach Science Publishers, New York.

Shincy, V.S. and Ghosh, S. (2021). A novel Sliding Mode-based guidance for soft landing of a spacecraft on an asteroid. In *AIAA Scitech 2021 Forum*. American Institute of Aeronautics and Astronautics.

Shincy, V.S. and Ghosh, S. (2022). Sliding-Mode-Control–based instantaneously optimal guidance for precision soft landing on asteroid. *Journal of Spacecraft and Rockets*.

Wibben, D.R. and Furfaro, R. (2016). Optimal sliding guidance algorithm for mars powered descent phase. *Advances in Space Research*, 57.

Wie, B. (1998). *Space vehicle dynamics and control*. AIAA.

Zarchan, P. (2012). *Tactical and Strategic Missile Guidance, Sixth Edition*. American Institute of Aeronautics and Astronautics, Inc.

Zhang, Y., Guo, Y., Ma, G., and Zeng, T. (2017). Collision avoidance ZEM/ZEV optimal feedback guidance for powered descent phase of landing on mars. *Advances in Space Research*, 59.

Zhou, L. and Xia, Y. (2014). Improved ZEM/ZEV feedback guidance for mars powered descent phase. *Advances in Space Research*, 54.